Polymer 54 (2013) 6381–6388

Contents lists available at ScienceDirect

Polymer

journal homepage: www.elsevier.com/locate/polymer

Autonomic self-healing in covalently crosslinked hydrogels containing hydrophobic domains

Deniz C. Tuncaboylu [a], Aslihan Argun [b], Melek Pamuk Algi [b], Oguz Okay [b],*

[a] *Bezmialem Vakif University, Faculty of Pharmacy, 34093 Istanbul, Turkey*
[b] *Istanbul Technical University, Department of Chemistry, Maslak, 34469 Istanbul, Turkey*

ARTICLE INFO

Article history:
Received 29 July 2013
Received in revised form
20 September 2013
Accepted 25 September 2013
Available online 2 October 2013

Keywords:
Self-healing
Hybrid gels
Hydrophobic associations

ABSTRACT

Self-healing hydrogels suffer from low mechanical strength due to their reversible breakable bonds which may limit their use in any stress-bearing applications. This deficiency may be improved by creating a hybrid network composed of a combination of a physical network formed via reversible crosslinks and a covalent network. Here, we prepared a series of hybrid hydrogels by the micellar copolymerization of acrylamide with 2 mol % stearyl methacrylate (C18) as a physical crosslinker and various amounts of *N*,*N*′-methylenebis(acrylamide) (BAAm) as a chemical crosslinker. Rheological measurements show that the dynamic reversible crosslinks consisting of hydrophobic associations surrounded by surfactant micelles are also effective within the covalent network of the hybrid hydrogels. A significant enhancement in the compressive mechanical properties of the hybrid gels was observed with increasing BAAm content. The existence of an autonomous self-healing process was also demonstrated in hybrid gels formed at low chemical crosslinker ratios. The largest self-healing efficiency in hybrids was observed in terms of the recovered elastic modulus, which was about 80% of the original value.

1. Introduction

Synthetic hydrogels are very similar to biological tissues, and therefore have been important materials for drug delivery and tissue engineering. Inspired by natural healing processes [1–3], a variety of synthetic hydrogels have been developed recently that can heal damage autonomously or by using an external stimulus such as temperature and pH [4–25]. Autonomous damage repair and resulting healing in such hydrogels require reversible breakable bonds which prevent the fracture of the molecular backbone. Different reversible molecular interactions have been used to generate self-healing hydrogels, including hydrogen bonding [4–8], electrostatic interactions [9–11], molecular recognition [12–14], metal coordination [15,16], π–π stacking [17], and dynamic chemical bonds [18–21]. However, self-healing of permanently crosslinked hydrogels is a challenging task because of the irreversible nature of chemical crosslinks. Phadke et al. achieved self-healing in chemically crosslinked hydrogels through introduction of pendant side chains possessing an optimal balance of hydrophilic and hydrophobic moieties [4]. Sun et al. prepared such dual gels by mixing two types of crosslinked polymer: ionically crosslinked alginate, and covalently crosslinked polyacrylamide (PAAm) [11].

Our group recently developed a simple strategy to create strong hydrophobic interactions between hydrophilic polymers leading to the production of self-healing hydrogels [22–25]. Large hydrophobes such as stearyl methacrylate (C18) could be copolymerized with the hydrophilic monomer acrylamide (AAm) in aqueous sodium dodecyl sulfate (SDS) solutions. This was achieved by the addition of salt (NaCl) into the reaction solution [22]. Salt leads to micellar growth and hence, solubilization of large hydrophobes within the grown wormlike SDS micelles. Incorporation of hydrophobic sequences within the hydrophilic polyacrylamide (PAAm) chains via micellar polymerization technique generates strong hydrophobic interactions, which prevent dissolution of the physical gels in water, while the dynamic nature of the junction zones provides homogeneity and self-healing properties. It was shown that the hydrophobic associations surrounded by surfactant micelles act as reversible breakable crosslinks, which are responsible for rapid self-healing of the hydrogels at room temperature without the need for any stimulus or healing agent [23–25].

Self-healing hydrogels synthesized so far suffer from low mechanical strength due to their reversible bonds which may limit their use in any stress-bearing applications. This deficiency may be improved by creating a hybrid network composed of a combination

---

* Corresponding author. Tel.: +90 212 2853156; fax: +90 212 2856386.
E-mail address: okayo@itu.edu.tr (O. Okay).

0032-3861/$ – see front matter © 2013 Elsevier Ltd. All rights reserved.
http://dx.doi.org/10.1016/j.polymer.2013.09.051

of a physical network formed via reversible breakable crosslinks and a covalent network. This type of hybrid approach has been used by several research groups to improve the mechanical performance of hydrogels [26–30], but not to create self-healing ability in a covalently crosslinked network. Here, we prepared a series of hybrid hydrogels by the micellar copolymerization of AAm with 2 mol % C18 as a physical crosslinker and various amounts of *N*,*N*′-methylenebis(acrylamide) (BAAm) as a chemical crosslinker. The rheological and mechanical properties as well as the self-healing abilities of the hybrid gels were investigated as a function of the chemical crosslinker ratio. As will be seen below, an enhancement in the compressive mechanical properties of the hybrid gels was observed with increasing BAAm content. We also demonstrate the existence of an autonomous self-healing process in hybrid gels formed at low chemical crosslinker ratios.

2. Experimental part

2.1. Materials

Acrylamide (AAm, Merck), *N*,*N*′-methylenebis(acrylamide) (BAAm, Merck), sodium dodecyl sulfate (SDS, Merck), ammonium persulfate (APS, Sigma), *N*,*N*,*N*′,*N*′-tetramethylethylenediamine (TEMED, Sigma), and NaCl (Merck) were used as received. Commercially available stearyl methacrylate (C18, Sigma) consists of 65% *n*-octadecyl methacrylate and 35% *n*-hexadecyl methacrylate. Hydrogels were prepared by the micellar copolymerization of AAm with C18 at 24 ± 1 °C for 24 h in the presence of an APS (3.5 mM) – TEMED (0.25 v/v %) redox initiator system. Following parameters were fixed:

Total monomer (acrylamide + C18) concentration	: 10 w/v %
C18 content of the monomer mixture	: 2 mol %
SDS concentration	: 7 w/v % (0.24 M)
NaCl concentration	: 0.5 M

BAAm as a chemical crosslinker was included into the comonomer feed at various crosslinker ratios X (molar ratio of BAAm to the monomer) between 0 and 0.02. The gel preparation condition was the same as that used for the preparation of the physical gels [22,23]. Shortly, SDS (0.7 g) was dissolved in 9.9 mL aqueous solution of NaCl (0.2925 g) at 35 °C to obtain a transparent solution. Then, hydrophobic monomer C18 (0.0862 g) was dissolved in this SDS–NaCl solution under stirring for 2 h at 35 °C. After addition and dissolving AAm (0.9137 g) and BAAm (between 0 and 40.4 mg) for 30 min, TEMED (25 μL) was added into the solution. Finally, 0.1 mL of APS stock solution (0.8 g APS/10 mL distilled water) was added to initiate the reaction. For the mechanical and gel fraction measurements, the copolymerization reactions were carried out in plastic syringes of 4.7 mm internal diameters while, for the rheological measurements, they were conducted within the rheometer. For comparison, chemical PAAm gels were also prepared under the same experimental conditions, but in the absence of C18 and SDS–NaCl system.

For the gel fraction measurements, hydrogel samples were immersed in a large excess of water at 24 °C for at least 30 days by replacing water every second or third day, until the SDS concentration in the external solution decreases below the detection limit of the methylene blue method (0.20 mg L^{-1}) [22,23]. Then, the equilibrium swollen gel samples were taken out of water and freeze dried. The gel fraction W_g, that is, the conversion of monomers to the crosslinked polymer (mass of water-insoluble polymer/initial mass of the monomer) was calculated from the masses of dry polymer network and from the comonomer feed.

2.2. Rheological experiments

Gelation reactions were carried out at 25 °C within the rheometer (Gemini 150 Rheometer system, Bohlin Instruments) equipped with a cone-and-plate geometry with a cone angle of 4° and diameter of 40 mm. The instrument was equipped with a Peltier device for temperature control. The reactions were monitored at an angular frequency ω of 6.3 rad/s and a deformation amplitude $\gamma_o = 0.01$. After a reaction time of 3 h, the elastic G' and viscous moduli G'' of the reaction solutions approached limiting values. Then, frequency-sweep tests were carried out at 25 °C, as described before [22].

2.3. Mechanical tests

The measurements were performed in a thermostated room at 24 ± 1 °C on cylindrical hydrogel samples of 4.7 mm diameter. The uniaxial compression measurements were performed on a Zwick Roell test machine using a 500 N load cell. The hydrogel sample of 5.3 ± 0.3 mm length was placed between the plates of the instrument. Before the test, an initial compressive contact to 0.004 ± 0.003 N was applied to ensure a complete contact between the gel and the plates. The tests were conducted at a strain rate of 1.6×10^{-3} s^{-1} (0.5 mm/min). Load and displacement data were collected during the experiment. Compressive stress was presented by its nominal σ_{nom} and true values σ_{true} ($=\lambda\ \sigma_{nom}$), which are the forces per cross-sectional area of the undeformed and deformed gel specimen, respectively, while the strain is given by λ, the deformation ratio (deformed length/initial length). Compressive modulus was calculated from the slope of stress–strain curves between 5 and 15% compressions. Cyclic compression tests were conducted at a constant crosshead speed of 0.5 mm/min to a maximum compression ratio, followed by retraction to zero force and a waiting time of 7 min, until the next cycle of compression. For reproducibility, at least six samples were measured for each gel and the results were averaged.

At large compressions, failure was not easily observed in hybrid gels formed at a crosslinker ratio $X < 0.01$ because the nominal stress σ_{nom} did not decrease after the samples broke. This is illustrated in Fig. 1 showing the stress–strain curves of hybrid gels under compression as the dependence of nominal σ_{nom} and true σ_{true} stresses on the deformation ratio λ. Although σ_{nom} increases continuously with increasing strain, $\sigma_{true} - \lambda$ plots pass through maxima due to the onset of failure in the gel specimen. This behavior observed at low crosslinker ratios was a consequence of the sample breaking into several pieces that still supported the stress. However, the gel sample that was brittle at a high crosslinker ratio suddenly fractures so that the point of failure was clear. The fracture stress σ_f and the compression ratio at break λ_f were calculated from the maxima in $\sigma_{true} - \lambda$ plots taken as the fracture point of the gel samples. Fig. 1 also shows that the use of $\sigma_{nom} - \lambda$ plots to assess gel fracture may lead to erroneously high fracture stresses σ_f, while our idea to assess σ_f from $\sigma_{true} - \lambda$ plots corrects this error. However, to make a comparison possible with previous works on self-healing hydrogels, we report in the following $\sigma_{nom} - \lambda$ plots up to the fracture point and the nominal fracture stresses.

The uniaxial elongation measurements were performed on a Zwick Roell test machine using a 10 N load cell under the following conditions: Strain rate = 0.075 s^{-1} (50 mm/min), sample length between jaws = 11 ± 1 mm. Samples were held on the test machine between clamps altered with anti-slip tape (Tesa, 25 × 15 mm) together with wood strips to better grip the slippery gel samples.

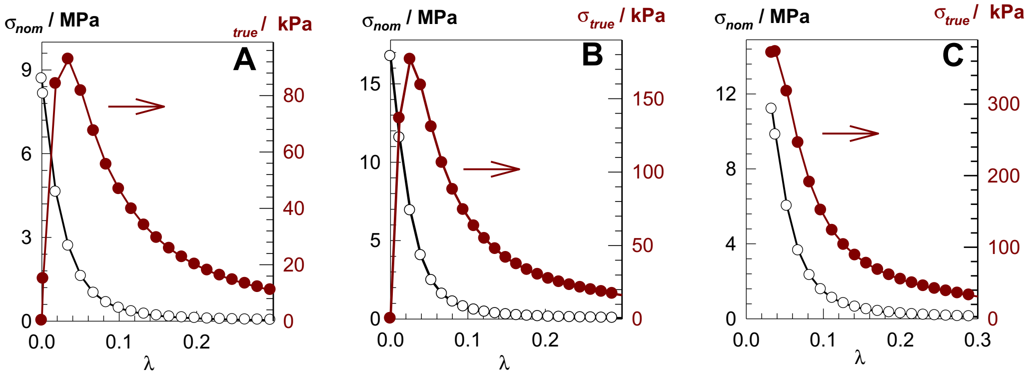

Fig. 1. Stress–strain curves of hybrid gels under compression as the dependence of nominal σ_{nom} (open symbols) and true σ_{true} stresses (filled symbols) on the deformation ratio λ. $X = 0.002$ (A), 0.005 (B), and 0.010 (C).

Cyclic elongation tests were conducted similar to the cyclic compression tests at a constant crosshead speed of 50 mm/min. We have to note that the tensile tests were conducted at a higher strain rate compared to the compression tests to prevent drying of the gel samples exhibiting a high stretchability.

3. Results and discussion

Hybrid gels were prepared by the micellar copolymerization of AAm with 2 mol % C18 as a physical crosslinker together with the chemical crosslinker BAAm at various crosslinker ratios X (molar ratio of BAAm to the monomer) between 0 and 0.02. The gel fraction W_g was unity for all the hydrogels indicating complete conversion of the monomers into the hybrid network. In the following, all the hydrogels investigated are at the state of preparation. Fig. 2A and B shows the frequency dependencies of the elastic modulus G' and the loss factor tan δ ($= G''/G'$) of the hydrogels formed at various X, respectively. The arrows show the directions of increasing X. In comparison, open symbols in the figures represent the data obtained from a chemical PAAm gel formed at $X = 0.02$ in the absence of C18. In contrast to the chemical gel that exhibits a frequency-independent elastic modulus G', hybrid gels exhibit frequency-dependent elastic moduli with plateau moduli at high frequencies ($>10^2$ rad/s). The height of the plateau increases with rising X due to the effect of covalent crosslinks on the elasticity of hybrid gels. At $X = 0.02$, the plateau elastic modulus of the hybrid is 25 kPa as compared to 20 kPa of the chemical gel, revealing the contribution of hydrophobic associations to the effective crosslink density of the hybrid gel at short experimental time scales. At longer times, the modulus of hybrids becomes less frequency-dependent with rising X, while the loss factor tan δ decreases demonstrating increasing lifetime of hydrophobic associations within the covalent network structure. At low frequencies, G' of the hybrid gel formed at $X = 0.02$ is less than G' of the chemical gel indicating that the presence of the hydrophobes and/or surfactant micelles affects the polymerization kinetics. Moreover, the peak in tan δ appears at around 10 rad/s independent of X indicating that the energy dissipation mainly occurs at this frequency for all the hybrid gels. The fact that all hybrids show time-dependent moduli reveals the finite lifetimes of C18 associations. Hence, the dynamic reversible crosslinks are also effective within the covalent network of the present hybrid hydrogels.

The mechanical behavior of the hydrogels was investigated by both uniaxial compression and tensile tests. Fig. 3A compares the stress–strain data of the hybrid gel formed at $X = 0.01$ with its individual components, the physical ($X = 0$) and chemical gels ($X = 0.01$), as the dependence of the nominal stress σ_{nom} on the deformation ratio λ. Fig. 3B shows a summary of the compressive fracture stresses σ_f, compressive moduli E, and the elongation ratios at break λ_f for each type of hydrogel. The hybrid gel withstands 8.1 ± 1 MPa compressive stress which is more than 24 and 4 times higher than that of the individual chemical and physical gels,

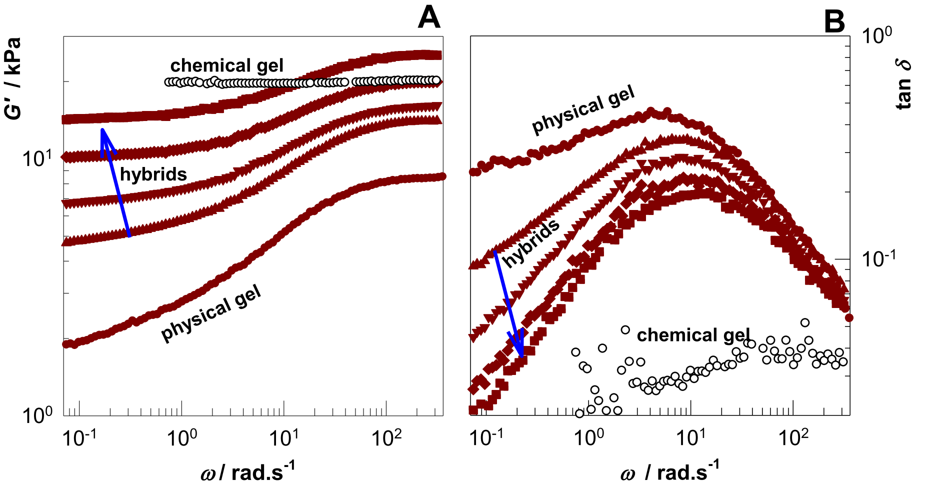

Fig. 2. G' (A) and tan δ (B) of hybrid gels at 25 °C shown as a function of angular frequency ω. $\gamma_o = 0.01$. The arrows show the directions of increasing crosslinker ratio X, which is 0 (●), 0.002 (▲), 0.005 (▼), 0.010 (◆), and 0.020 (■). Open symbols represent data obtained from a chemical PAAm gel formed at $X = 0.02$.

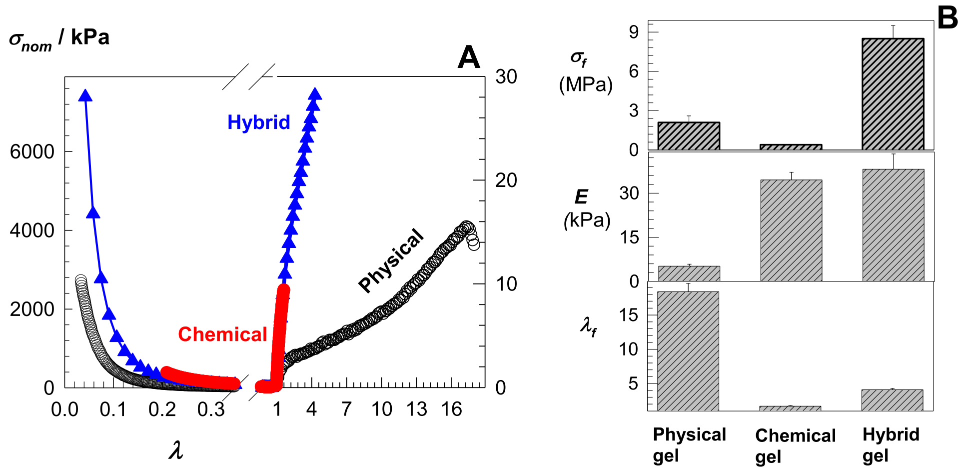

Fig. 3. (A): Typical stress–strain curves of the physical (○), chemical (●), and hybrid gels (▲) under compression ($\lambda < 1$) and elongation ($\lambda > 1$) as the dependence of nominal stress σ_{nom} on the deformation ratio λ. (B): Fracture stress σ_f, compressive modulus *E* and elongation ratio at break λ_f for the physical, chemical ($X = 0.01$) and hybrid gels ($X = 0.01$).

respectively. Thus, the fracture stress of the hybrid gel far exceeds that of either of its parents. The modulus of the hybrid is 38 ± 5 kPa, which is the sum of the moduli of the chemical and physical gels (35 ± 1 kPa and 5 ± 1 kPa, respectively). Thus, the mechanical strength of the physical gel is significantly improved by use of the hybrid approach. In contrast, the hybrid gel does not exhibit the high stretchability of the physical gel. As seen in Fig. 3, although the physical gel ruptures when stretched to about 18 times its original length, the hybrid gel ruptures at $\lambda_f = 4.1 \pm 0.2$, which is only 2.4 times higher than that of the chemical gel (1.7 ± 0.1).

Fig. 4A represents stress–strain data of the hybrid gels formed at various *X* between 0.002 and 0.02. In Fig. 4B, mechanical characteristics of the gels are plotted against the crosslinker ratio *X*. The results obtained from the chemical gels formed at $X = 0.01$ and 0.02 are also shown by triangles. The general trend is that the hybrid gels formed at $X < 0.02$ withstand up to 96–97% compression ratios and exhibit an increase in the fracture stress σ_f with increasing *X*, while those formed at larger *X* become brittle. Moreover, the modulus *E* increases while the elongation at break λ_f decreases continuously with rising *X* and, the values *E* and λ_f of hybrids are mainly determined by the chemical gel component.

Fig. 4B also shows that the elongation at break drastically decreases upon addition of a small amount of the chemical crosslinker BAAm. For instance, the physical gel ($X = 0$) withstands up to an elongation ratio of 18 ± 1, whereas the hybrid with $X = 0.002$ fails at an elongation ratio of 8. Since the crosslinker ratio $X = 0.002$ corresponds to one crosslinker per 500 monomers, i.e., on average 250 units between two successive covalent crosslinks, the network chains are expected to be long enough to behave like Gaussian coils. For a network of Gaussian chains, the maximum extensibility λ_m is equal to $N^{1/2}$, where *N* is the number of monomer units between two successive crosslinks, i.e., $N = (2X)^{-1}$ [31]. Thus, for $X = 0.002$, λ_m is predicted to be 16, which is close to λ_f of the physical gel. However, mixing these chemical and physical crosslinks to make a hybrid gel results in a decrease of λ_f to 8 indicating that even a loosely crosslinked covalent network structure leads to a dramatic loss of stretchability of the physical gel.

To understand the enhancement in compressive mechanical properties of the physical gel in spite of loss of its extensibility upon addition of chemical crosslinks, it is important to consider the characteristics of PAAm gels formed by BAAm crosslinker. Such gels possess an uneven topological distribution of crosslinks, commonly

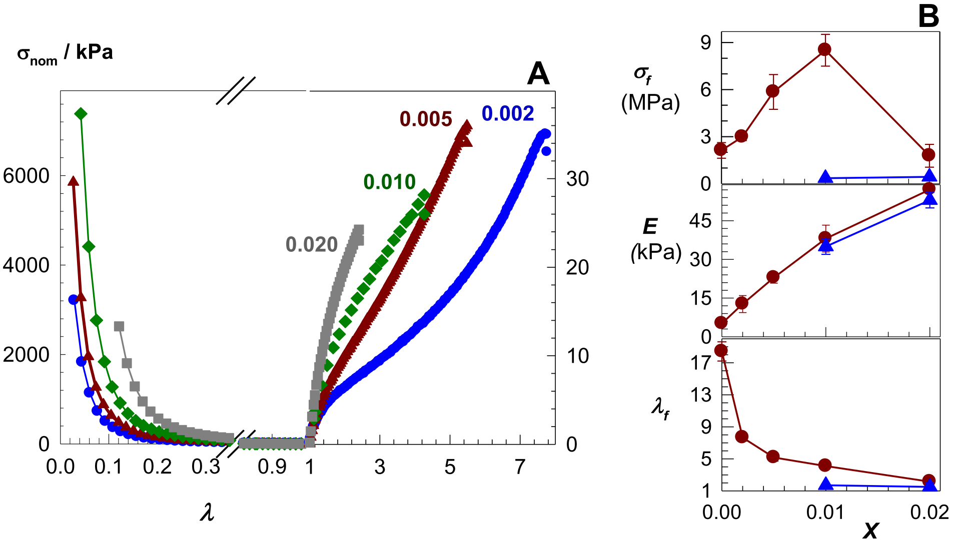

Fig. 4. (A): Typical stress–strain curves of the hybrid gels formed at various crosslinker ratios *X* indicated. (B): Fracture stress σ_f, compressive modulus *E*, and the elongation ratio at break λ_f of the gels plotted against the crosslinker ratio *X*. The data of the chemical gels are shown by triangles.

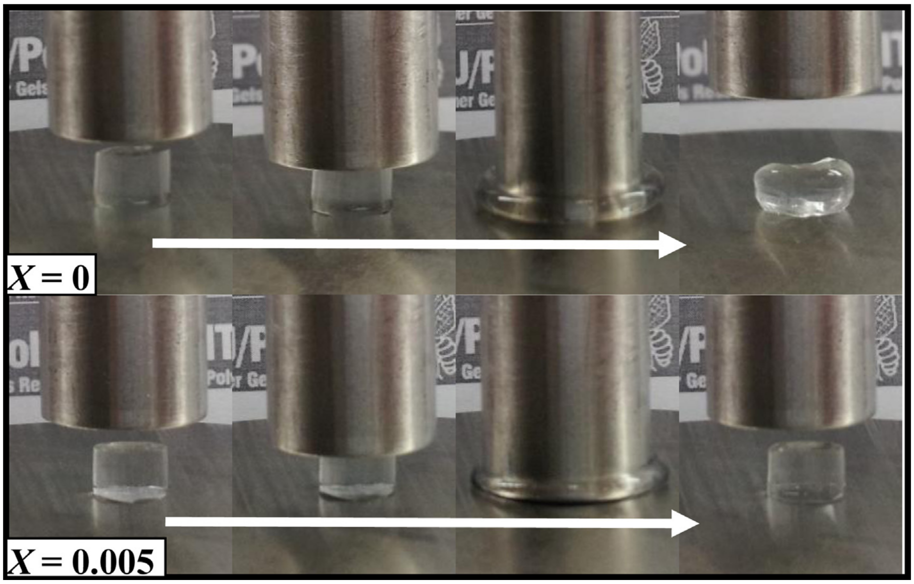

Fig. 5. Photographs of the physical ($X = 0$) and hybrid gels ($X = 0.005$) during the compression tests. The physical gel remains deformed after removal of the stress (top-right image) and, a full recovery of the original shape was observed after a waiting time of 3 min.

referred to as spatial gel inhomogeneity [32,33], a feature that is caused by cyclization reactions, microgel formation during gelation, differences between the reactivities of vinyl groups, and diffusion controlled reactions [32–38]. To highlight the imperfections in the covalent network structure of the hybrids, we estimated the efficiency of BAAm to form elastically effective crosslinks. Since the elastic modulus G' of the chemical gel formed at $X = 0.02$ is independent of the frequency (Fig. 2A), it also corresponds to its shear modulus G. Assuming that all BAAm molecules used in the gel preparation participate in forming effective crosslinks, theoretical shear modulus $G_{\rm theo}$ of the hydrogel can be estimated as [38]:

$$G_{\rm theo} = A\frac{1}{NV_{\rm r}}RT\nu_2^0 \tag{1}$$

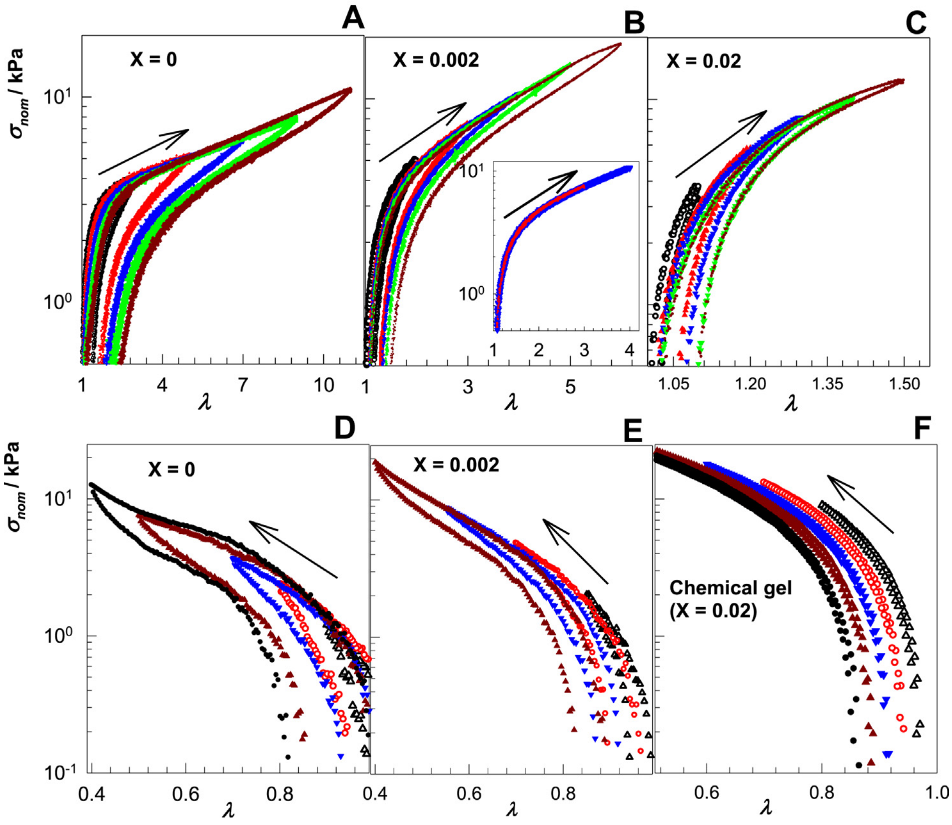

Fig. 6. Nominal stress $\sigma_{\rm nom}$ vs deformation ratio λ curves from cyclic elongation (A–C) and compression tests (D–F) for the gel samples with various X indicated. For comparison, the behavior of a chemical PAAm gel ($X = 0.02$) is shown in the lower right figure. The tests were conducted with increasing strain.

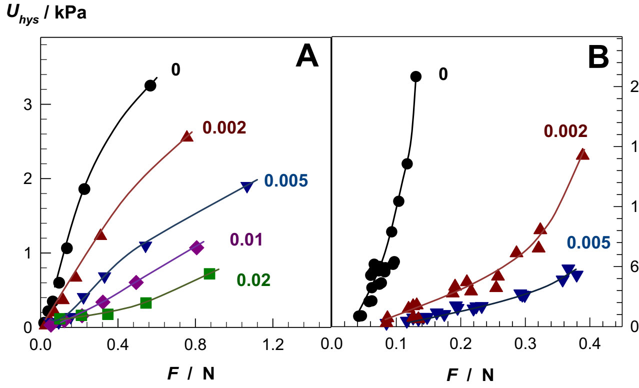

Fig. 7. Hysteresis energy U_{hys} during the loading/unloading compression (A) and elongation tests (B) shown as a function of the maximum load F. The crosslinker ratio X as indicated. Due to the limited extensibility of the gels, data of only two hybrid gels are shown in B.

where the front factor A equals to 1 for an affine network and $1 - 2/\phi$ for a phantom network, ϕ is the functionality of the crosslinks, V_r is the molar volume of repeat unit (53 mL/mol), ν_2^0 is the volume fraction of crosslinked polymer after the gel preparation. R and T are in their usual meanings. Previous works show that the phantom network theory of elasticity adequately describes the stress–strain behavior of PAAm gels [39]. Assuming phantom network behavior ($\phi = 4$), G_{theo} of the chemical gel with $X = 0.02$ was calculated as 70 kPa, as compared to its experimental value of 25 kPa. Thus, about 64% of BAAm used in the gel preparation were wasted in elastically ineffective links. For the chemical gel formed at $X = 0.002$, the modulus was measured as 3.3 kPa as compared to $G_{theo} = 7$ kPa, i.e., the wasted fraction of BAAm is 53%. The high fraction of wasted BAAm in PAAm gels mainly originates from the multiple crosslinking reactions leading to an inhomogeneous distribution of crosslinks along the gel sample, i.e., to a broad molecular weight distribution of the network chains [34,35]. Although the small strain properties such as the modulus would be expected to be dominated by the contribution of both long and short network chains, the extensibility of the network chains before failure will mainly be influenced by the shorter chains. The loss of stretchability of the physical gel upon addition of chemical crosslinks is thus due to the contribution of short network chains. Since increasing chemical crosslink density also increases the degree of inhomogeneity [32,33,36–38], increasing number of shorter network chains make the hybrid gels brittle at crosslinker ratios $X > 0.01$. On the other hand, the improvement in the compressive mechanical properties of hybrids is due to the introduction of a covalent network structure. This feature is also illustrated in Fig. 5 where the images of the physical ($X = 0$) and hybrid gels ($X = 0.005$) during the compression tests are shown. Hybrid gel is highly elastic due to the presence of permanent crosslinks and recovers back to its original shape when the stress is released. In contrast, the physical gel remains deformed after removal of the stress (the top-right image in Fig. 5) and, a full recovery of the original shape was observed after a waiting time of 3 min.

Cyclic mechanical testing is a powerful tool to understand the nature of crosslinks in the hybrid gels. Five successive loading–unloading compression and tensile cycles of hybrid gels up to a strain below the failure are shown in Fig. 6. The tests were carried out with increasing maximum strain and with a waiting time of 7 min between cycles. For clarity, successive cycles are presented by curves with different colors and the loading curves are indicated by up arrows. For comparison, the behavior of the chemical PAAm gel ($X = 0.02$) is also shown in figure (Fig. 6F). Due to the lack of an efficient energy dissipation mechanism, the chemical gel exhibits negligible hysteresis across the entire measured range of strains whereas the physical gel ($X = 0$, left panel) exhibits a significant hysteresis. The energy U_{hys} dissipated during the cycle was calculated from the area between the loading and unloading curves. Since hydrophobic associations can be broken under low external forces while the chemical crosslinks remain intact, we calculated U_{hys} released under a maximum load F of less than 1 N. In Fig. 7, the hysteresis energies U_{hys} calculated during compression and tensile cycles are plotted against F for various crosslinker ratios X. The hysteresis increases with increasing maximum load F, i.e., with increasing maximum strain during the loading step. Moreover, as the crosslinker ratio X is increased at a constant load, hysteresis decreases indicating decreasing number of hydrophobic associations acting as reversibly breakable crosslinks.

The perfect superposition of the successive loading curves of the physical gel demonstrates that the damage done to this gel sample during the loading cycle is recoverable in nature. Although at a lesser extent, this reversibility is also observable in the hybrid hydrogel formed at $X = 0.002$. As illustrated in the inset to Fig. 6B,

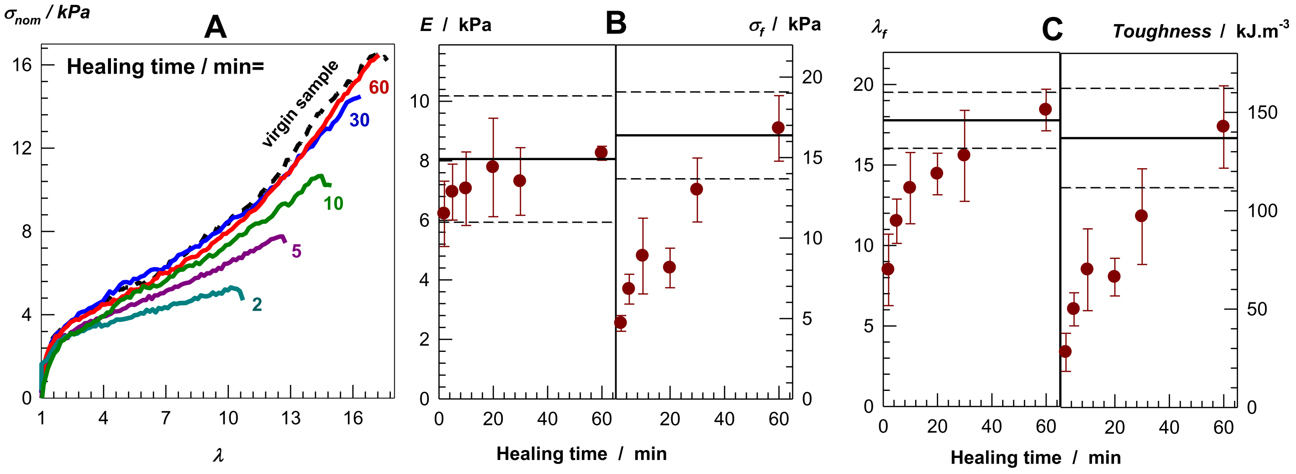

Fig. 8. (A): Stress–strain curves of virgin (dashed curve) and healed gel samples with $X = 0$ (solid curves). Healing times are indicated. (B, C): Tensile modulus E, tensile fracture stress σ_f, elongation ratio λ_f at break, and toughness of healed gels shown as a function of the healing time. The solid lines represent the behavior of virgin gel sample and the dashed lines are the standard deviations.

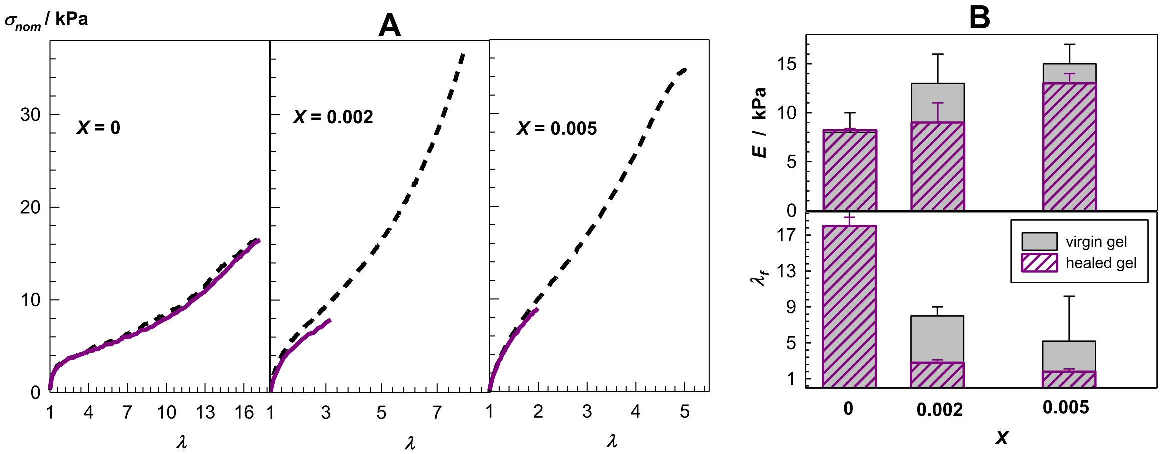

Fig. 9. (A): Stress–strain curves of virgin (dashes curves) and healed gel samples (solid curves). The crosslinker ratio X of the gels is indicated. Healing time = 60 min. (B): Tensile modulus E and the elongation ratio at break λ_f of virgin and healed gel samples shown as a function of the crosslinker ratio X.

the loading curve with a maximum strain $\lambda_{max} = 4$ closely follows the path of the previous loading curve with $\lambda_{max} = 3$ implying that the structure of the hybrid gel returns to its initial state after the cycle up to $\lambda_{max} = 3$ and the energy U_{hys} released during this cycle is due to the recoverable damage of the physical crosslinks. For $\lambda_{max} = 3$, U_{hys} was calculated as 2.14 kPa for this hybrid gel, as compared to 2.69 kPa for the physical gel subjected to the same cycle. Since the hysteresis energy is proportional to the number of associations broken down during the cycle [23,24], this means that about 80% of the hydrophobic associations in the hybrid gel are broken reversibly during deformation.

Experiments showed that, when the fracture surfaces of a ruptured hybrid gel sample with $X < 0.01$ are pressed together at 24 °C, the two pieces merge into a single piece. This demonstrates autonomous self-healing in a covalently crosslinked hydrogel. To quantify the healing efficiency, tensile testing experiments were performed using cylindrical gel samples of 4.7 mm in diameter and 6 cm in length. The samples were cut in the middle and then, the two halves were merged together within a plastic syringe (of the same diameter as the gel sample) at 24 °C by slightly pressing the piston plunger. To find the optimum healing time, we first conducted the mechanical measurements using the physical gel ($X = 0$) at various healing times. In Fig. 8A, stress–strain curves of the virgin (dashed curve) and healed gel samples (solid curves) are shown. In Fig. 8B and C, the tensile modulus E, the fracture stress σ_f, the elongation ratio at break λ_f and the toughness of the healed gel samples are plotted against the healing time. The horizontal solid lines represent the characteristics of the virgin gel with standard deviations indicated by the dashed lines. The fracture stress after 10 min healing is ~10 kPa which is 63% of the fracture stress of the virgin gel sample. The results indicate the occurrence of a rapid and autonomous self-healing process in the physical gel. A healing time of 60 min suffices to recover all the initial mechanical properties of the physical hydrogel.

Self-healing tests were also performed using hybrid gel samples after a healing time of 60 min which was the optimum time for the physical gel. No self-healing was observed in hybrids formed at $X \geq 0.01$, which is attributed to decreased mobility of C18 blocks in the inhomogeneous network structure. However, those formed at lower crosslinker ratios exhibited self-healing behavior. In Fig. 9, the stress–strain curves (A), the tensile moduli E (B), and the elongation ratios at break λ_f (C) of the virgin and healed gel samples are shown for $X = 0$, 0.002, and 0.005. The largest healing efficiency in hybrids was observed in terms of the recovered tensile modulus E, which was about 80% of the original value. We have to mention that the tensile moduli of the original gels are 8, 13, and 15 kPa for $X = 0$, 0.002, and 0.005, respectively. Thus, the physical crosslinks contribute 53–62% of the moduli of these hybrid gels, which seem to be responsible for the high recovery of E of the healed gel samples. The healed gel samples formed at $X = 0.002$ and 0.005 withstand up to 9 kPa fracture stress at 200% deformation ratios. The results thus show that 30 ± 5% of the tensile fracture stress and the elongation at break of the virgin samples can be autonomously recovered in the hybrid gels formed at $X \leq 0.005$.

4. Conclusions

Self-healing hydrogels suffer from low mechanical strength due to their reversible breakable bonds. Here, we attempted to improve this deficiency by creating a hybrid network composed of a combination of a physical network formed via reversible crosslinks and a covalent network. We prepared a series of hybrid hydrogels by the micellar copolymerization of AAm with 2 mol % C18 as a physical crosslinker and various amounts of BAAm as a chemical crosslinker. Rheological measurements show that the dynamic reversible crosslinks consisting of hydrophobic associations surrounded by surfactant micelles are also effective within the covalent network of the hybrid hydrogels. A significant enhancement in the compressive mechanical properties of the hybrid gels was observed with increasing BAAm content. For instance, the hybrid gel formed at $X = 0.01$ withstands 8.1 ± 1 MPa compressive stress which is more than 24 and 4 times higher than that of the individual chemical and physical gels, respectively. The modulus of the hybrid gel formed at $X = 0.01$ is 38 ± 5 kPa, which is the sum of the moduli of the chemical and physical gels. In contrast, the hybrid gel does not exhibit the high stretchability of the physical gel. Cyclic tensile and compression tests show that the fraction of hydrophobic associations reversibly broken under an external force decreases with increasing crosslinker ratio X. The largest self-healing efficiency in hybrids was observed in terms of the recovered modulus E, which was about 80% of the original value. The healed gel samples formed at a low BAAm content withstand about 9 kPa fracture stress at 200% deformation ratios.

The results also show that self-healing in hybrid gels can be observed at low chemical crosslink densities where the network chains are sufficiently flexible to allow the re-formation of broken hydrophobic associations on the cut surfaces. Recently, Phadke et al. have demonstrated pH-induced healing in chemical gels containing dangling hydrocarbon side chains with terminal carboxyl groups that mediate hydrogen bonding across the hydrogel interfaces at a low pH [4]. They also showed that healing requires a low crosslink density to make the carboxyl groups across the damaged area available to each other [4]. Thus, our results also support this finding. Moreover, a lesser degree of spatial gel inhomogeneity is expected to produce much better healing efficiencies in hybrid hydrogels. We also propose that the use of hydrophobic monomers with longer alkyl side chains would produce enhanced self-healing properties due to the increased mobility of the hydrophobes.

Acknowledgment

Work was supported by the Scientific and Technical Research Council of Turkey (TUBITAK), TBAG – 109T646. M. P. A. acknowledges the financial support from TUBITAK for a post-doctoral scholarship. O. O. thanks Turkish Academy of Sciences (TUBA) for the partial support.

References

[1] Fantner GE, Oroudjev E, Schitter G, Golde LS, Thurner P, Finch MM, et al. Biophys J 2006;90:1411–8.
[2] Hamilton AR, Sottos NR, White SR. Adv Mater 2010;90:5159–63.
[3] Fratzl P. J R Soc Interface 2007;4:637–42.
[4] Phadke A, Zhang C, Arman B, Hsu C-C, Mashelkar RA, Lele AK, et al. Proc Natl Acad Sci 2012;109:4383–8.
[5] Zhang H, Xia H, Zhao Y. ACS Macro Lett 2012;1:1233–6.
[6] Cui J, del Campo A. Chem Commun 2012;48:9302–4.
[7] Liu J, Song G, He C, Wang H. Macromol Rapid Commun 2013;34:1002–7.
[8] Haraguchi K, Uyama K, Tanimoto H. Macromol Rapid Commun 2011;32:1253–8.
[9] South AB, Lyon LA. Angew Chem Int Ed 2010;49:767–71.
[10] Wang Q, Mynar JL, Yoshida M, Lee E, Lee M, Okura K, et al. Nature 2010;463:339–43.
[11] Sun J-Y, Zhao X, Illeperuma WRK, Chaudhuri O, Oh KH, Money DJ, et al. Nature 2012;489:133–6.
[12] Foo CTSWP, Lee JC, Mulyasasmita W, Parisi-Amon A, Heilshorn SC. Proc Natl Acad Sci 2009;106:22067–72.
[13] Appel EA, Biedermann F, Rauwald U, Jones ST, Zayed JM, Scherman OA. J Am Chem Soc 2010;132:14251–60.
[14] Skrzeszewska PJ, Sprakel J, Wolf FA, Fokkink R, Stuart MAC, van de Gucht J. Macromolecules 2010;43:3542–8.
[15] Holten-Andersen N, Harrington MJ, Birkedal H, Lee BP, Messersmith PB, Lee KYC, et al. Proc Natl Acad Sci 2011;108:2651–5.
[16] Shafiq Z, Cui J, Pastor-Perez L, San Miguel V, Gropeanu RA, Serrano C, et al. Angew Chem Int Ed 2012;124:4408–11.
[17] Xu Y, Wu Q, Sun Y, Bai H, Shi G. ACS Nano 2010;4:7358–62.
[18] Liu F, Li F, Deng G, Chen Y, Zhang B, Zhang J, et al. Macromolecules 2012;45:1636–45.
[19] Deng G, Tang C, Li F, Jiang H, Chen Y. Macromolecules 2010;43:1191–4.
[20] Zhang Y, Tao L, Li S, Wei Y. Biomacromolecules 2011;12:2894–901.
[21] He L, Fullenkamp DE, Rivera JG, Messersmith PB. Chem Commun 2011;47:7497–9.
[22] Tuncaboylu DC, Sari M, Oppermann W, Okay O. Macromolecules 2011;44:4997–5005.
[23] Tuncaboylu DC, Sahin M, Argun A, Oppermann W, Okay O. Macromolecules 2012;45:1991–2000.
[24] Tuncaboylu DC, Argun A, Sahin M, Sari M, Okay O. Polymer 2012;53:5513–22.
[25] Akay G, Hassan-Raesi A, Tuncaboylu DC, Orakdogen N, Abdurrahmanoglu S, Oppermann W, et al. Soft Matter 2013;9:2254–61.
[26] Abdurrahmanoglu S, Can V, Okay O. Polymer 2009;50:5449–55.
[27] Hao J, Weiss RA. Polymer 2013;54:2174–82.
[28] Rose S, Dizeux A, Narita T, Hourdet D, Marcellan A. Macromolecules 2013;46:4095–104.
[29] Miquelard-Garnier G, Hourdet D, Creton C. Polymer 2009;50:481–90.
[30] Miquelard-Garnier G, Creton C, Hourdet D. Soft Matter 2008;4:1011–23.
[31] Orakdogen N, Erman B, Okay O. Macromolecules 2010;43:1530–8.
[32] Shibayama M. Macromol Chem Phys 1998;199:1–30.
[33] Bastide J, Candau SJ. In: Cohen Addad JP, editor. Physical properties of polymeric gels. Wiley; 1996. p. 143.
[34] Okay O, Kurz M, Lutz K, Funke W. Macromolecules 1995;28:2728–37.
[35] Funke W, Okay O, Joos-Muller B. Adv Polym Sci 1998;136:139–234.
[36] Kizilay MY, Okay O. Polymer 2004;45:2567–76.
[37] Kizilay MY, Okay O. Macromolecules 2003;36:6856–62.
[38] Kizilay MY, Okay O. Polymer 2003;44:5239–50.
[39] Baker JP, Hong LH, Blanch HW, Prausnitz JM. Macromolecules 1994;27:1446–54.